EUROPHYSICS LETTERS 15 September 2002

Europhys. Lett., **59** (6), pp. 916–922 (2002)

Pattern formation during adhesion of multicomponent membranes

T. R. Weikl[1,3], J. T. Groves[2] and R. Lipowsky[3]

[1] *Department of Pharmaceutical Chemistry, University of California San Francisco, CA 94143-1204, USA*
[2] *Department of Chemistry, University of California - Berkeley, CA 94720, USA*
[3] *Max-Planck-Institut für Kolloid- und Grenzflächenforschung 14424 Potsdam, Germany*

(received 14 March 2002; accepted in final form 26 June 2002)

PACS. 87.16.Dg – Membranes, bilayers, and vesicles.
PACS. 64.75.+g – Solubility, segregation, and mixing; phase separation.
PACS. 89.75.Kd – Patterns.

Abstract. – The adhesion dynamics of multicomponent membranes containing specific receptors (stickers) and repulsive macromolecules (repellers) is studied theoretically. We find different dynamic regimes with clearly distinct patterns of stickers and repellers at intermediate times. The pattern formation is shown to depend critically on the strength of the repeller barrier which opposes sticker binding. For strong barriers composed of long repellers, the nucleation time for sticker binding is large compared to typical diffusion times, and the stickers bind by condensation around a single nucleus. For weaker repeller barriers, many nuclei are formed initially. Due to the diffusion of stickers into the adhesion area, nuclei at the rim of this area subsequently grow faster, which results in circular sticker patterns. At sufficiently high sticker concentrations, the pattern evolution is similar to recent observations during T cell adhesion.

Introduction. – The adhesion of cells plays a key role in important biological processes such as tissue development and immune response. The highly selective interactions leading to cell adhesion are mediated by a variety of specific receptors which are embedded in the cell membranes. The bound receptor-ligand pairs of opposing cells are often arranged into supramolecular patterns which show a complex evolution during cell adhesion [1–3]. For some biological processes, the formation of these patterns seems to be the central event leading to cell activation. For example, the immune response of T lymphocyte and natural killer cells to target cells is triggered by the formation of characteristic patterns at the cell-cell junction [1–3]. One possible explanation for the pattern formation during cell adhesion has been given in terms of active processes involving the cytoskeleton of the cells [4, 5]. More recently, it has been shown theoretically, using a detailed model for T lymphocyte adhesion, that such patterns may also result from spontaneous self-assembly processes [6], which possibly operate in concert with cytoskeletal activity in living cells.

In this letter, we consider a statistical mechanical model for the adhesion of multicomponent membranes with adhesive receptors (stickers) and repulsive macromolecules (repellers). We find distinct dynamic regimes of pattern formation depending on the characteristic lengths and the concentrations of stickers and repellers: (A) Long repellers impose a strong barrier to sticker adhesion. The nucleation time for sticker binding therefore is large compared to typical diffusion times, and the membrane binds via growth of a single sticker nucleus, as has been

recently observed for biomimetic vesicles with PEG-lipopolymers as repellers and integrins as stickers [7]. (B) For short repellers, the nucleation time for sticker binding is small, and many nuclei of bound stickers are formed initially. Due to the diffusion of stickers into the adhesion area, nuclei at the rim of this area grow faster, and at sufficiently high sticker concentrations, a ring of bound stickers is formed which encloses a central domain of repellers, see fig. 2 below. At later times, this pattern inverts, and a central sticker cluster is surrounded by repellers. The sequence of patterns in this regime has a striking similarity to the pattern evolution observed during T cell adhesion [2]. (C) In an intermediate regime, the sticker concentration is not large enough for the formation of a closed sticker ring from the initial nuclei. Instead, circular arrangements of separate sticker clusters emerge, see fig. 3 below.

General model. – First, we describe our membrane model which was previously used in order to determine the time-independent behavior of these systems in equilibrium [8–12]. The conformations of a multicomponent membrane in contact with a substrate are described by the field l for the local separation between membrane and substrate and by the concentration field n for the membrane composition [8]. It is convenient to discretize the substrate into a two-dimensional square lattice with lattice constant a. This discretization divides the membrane, which is on average parallel to the substrate, into square patches of size a^2. The sticker and repeller positions can then be given by occupation numbers n_i at the lattice sites i which adopt the value $n_i = 1$ for membrane patches with a sticker, $n_i = 2$ for patches with a repeller, and $n_i = 0$ for "neutral" patches without stickers or repellers. In terms of these variables, the canonical Hamiltonian can be written in the general form [8, 9]

$$\mathcal{H}\{l,n\} = \sum_i (\kappa/2a^2)(\Delta_{\rm d} l_i)^2 + \sum_i [V_{\rm hw}(l_i) + \delta_{1,n_i} V_{\rm s}(l_i) + \delta_{2,n_i} V_{\rm r}(l_i)] \qquad (1)$$

with the hard-wall potential $V_{\rm hw}(l_i) = \infty$ for $l_i \leq 0$ and $V_{\rm hw}(l_i) = 0$ for $l_i > 0$, and the Kronecker symbol $\delta_{i,j} = 1$ for $i = j$ and $\delta_{i,j} = 0$ otherwise. The first term represents the elastic energy of the membrane. For simplicity, the bending rigidity κ is assumed to be independent of the membrane composition. The discretized Laplacian $\Delta_{\rm d}$ is given by $\Delta_{\rm d} l_i = \Delta_{\rm d} l_{x,y} = l_{x+a,y} + l_{x-a,y} + l_{x,y+a} + l_{x,y-a} - 4l_{x,y}$. The second term of the Hamiltonian (1) represents the interaction energy between the membrane and the substrate. In the following, stickers and repellers are simply characterized by the interaction potentials

$$V_{\rm s}(l_i) = U_{\rm s}\theta(l_{\rm s} - l_i) \quad \text{and} \quad V_{\rm r}(l_i) = U_{\rm r}\theta(l_{\rm r} - l_i)\,, \qquad (2)$$

where the step function $\theta(x)$ is equal to 0 for $x < 0$ and equal to 1 for $x \geq 0$. For $U_{\rm s} < 0$ and $U_{\rm r} > 0$, the sticker potential $V_{\rm s}$ is a square-well potential with binding energy $|U_{\rm s}|$ and range $l_{\rm s}$, and the repeller potential $V_{\rm r}$ has a barrier of height $U_{\rm r}$ and range $l_{\rm r}$. In this letter, we will focus on the relatively large sticker and repeller energies $U_{\rm s} = -10T$ and $U_{\rm r} = 10T$, where T is the temperature in energy units.

Equilibrium phase behavior. – In this section, we consider the equilibrium behavior in order to determine the regions of the parameter space where phase separation occurs and, thus, pattern formation can be expected. It is convenient to start from the grand-canonical Hamiltonian corresponding to (1) which is obtained by adding the term $-\sum_i (\delta_{1,n_i}\mu_{\rm s} + \delta_{2,n_i}\mu_{\rm r})$. Here, $\mu_{\rm s}$ and $\mu_{\rm r}$ are the relative chemical potentials for sticker and repeller patches with respect to "neutral" patches. As shown in [8,9], the degrees of freedom of the concentration field n can be integrated out exactly in the partition function since the Hamiltonian (1) is linear in n. This leads to an effective membrane potential with a well for $0 < l_i < l_{\rm s}$ and a barrier of height $U_{\rm ba}$ for $l_{\rm s} < l_i < l_{\rm r}$, provided the repeller range $l_{\rm r}$ is larger than the sticker range $l_{\rm s}$. The effective

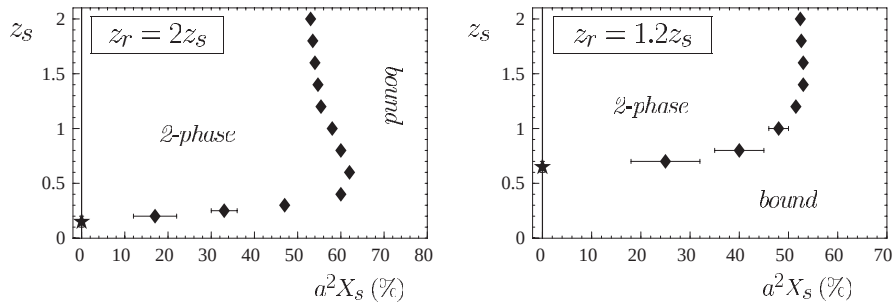

Fig. 1 – Phase diagrams for a multicomponent membrane as a function of the sticker concentration X_s and the rescaled potential ranges z_s and z_r of stickers and repellers. The chemical potential for the repellers is $\mu_\mathrm{r} = 0$, which corresponds to a repeller concentration $a^2X_\mathrm{r} = 0.5$ in the unbound phase. At large z_s and z_r, the repeller barrier with rescaled width $z_\mathrm{r} - z_\mathrm{s}$ is strong, which leads to lateral phase separation and 2-phase coexistence. The data points correspond to the sticker concentrations in the bound phase. The sticker contration $a^2X_\mathrm{s} \simeq 10^{-4}$ in the unbound phase is given by the vertical lines. The critical points as obtained from extrapolation are represented by stars.

barrier height is simply given by $U_\mathrm{ba} = T\ln(1 + e^{\mu_\mathrm{r}/T}/(1 + e^{\mu_\mathrm{s}/T})) \simeq T\ln(1 + e^{\mu_\mathrm{r}/T})$ in the limit of large sticker and repeller energies $|U_\mathrm{s}|$ and U_r. It follows from scaling arguments [10] that lateral phase separation occurs for strong barriers with

$$U_\mathrm{ba}(l_\mathrm{r} - l_\mathrm{s})^2 > ca^2T^2/\kappa\,, \tag{3}$$

where c is a dimensionless coefficient. The two coexisting phases are a bound phase with a higher sticker concentration, and an unbound phase with a larger repeller concentration. According to eq. (3), the tendency for lateral phase separation is weakened by an increase in the temperature T, in contrast to the fluctuation-induced mechanisms for phase separation in the case of rigid stickers [9], stickers with larger lateral size [11], or rigid inclusions [12]. Similar mechanisms for phase separation due to a potential barrier have been discussed in [13–15].

Here, we consider Monte Carlo (MC) simulations of the full model defined by eq. (1) in order to estimate the coefficient c in eq. (3). The corresponding phase diagrams are shown in fig. 1. In the simulations, we determine the sticker concentration $X_\mathrm{s} \equiv \langle\delta_{n_i,1}\rangle/a^2$ as a function of the chemical potential μ_s of the stickers. Lateral phase separation is reflected in a discontinuity of $X_\mathrm{s}(\mu_\mathrm{s})$ at a transition value $\mu_\mathrm{s} = \mu_\mathrm{s}^*$. The two limiting values of X_s at μ_s^* correspond to the sticker concentrations in the two coexisting phases and depend on the rescaled potential ranges $z_\mathrm{s} = (l_\mathrm{s}/a)\sqrt{\kappa/T}$ and $z_\mathrm{r} = (l_\mathrm{r}/a)\sqrt{\kappa/T}$ of the stickers and repellers, see fig. 1. The ratio of z_r and z_s is 2 for the left and 1.2 for the right diagram. The fixed chemical potential of the repellers is $\mu_\mathrm{r} = 0$, which corresponds to a repeller concentration $a^2X_\mathrm{r} \simeq e^{\mu_\mathrm{r}/T}/(1+e^{\mu_\mathrm{r}/T}) = 0.5$ in the unbound phase where the sticker concentration is small, see vertical lines. The strength of the repeller barrier with width $z_\mathrm{r} - z_\mathrm{s}$ decreases with z_s and z_r. The 2-phase coexistence regions become critical points at $z_\mathrm{s}^c = 0.15 \pm 0.05$ for $z_\mathrm{r} = 2z_\mathrm{s}$ and at $z_\mathrm{s}^c = 0.65 \pm 0.05$ for $z_\mathrm{r} = 1.2z_\mathrm{s}$. In agreement with eq. (3), the two values differ by a factor of 5 within the numerical accuracy reflecting the same critical barrier strength. From the two critical values, we conclude $c = 0.013 \pm 0.005$ for the coefficient in eq. (3).

Adhesion dynamics. – In order to study the time evolution of the adhesion process, we start from the canonical Hamiltonian (1) with fixed sticker and repeller concentrations X_s and X_r. We consider the following adhesion geometry: The contact area of the membrane is assumed to be a circle with diameter $100a$, where a is the lattice spacing. This circular contact area is surrounded by a membrane ring of width $50a$ in which the membrane is not in contact

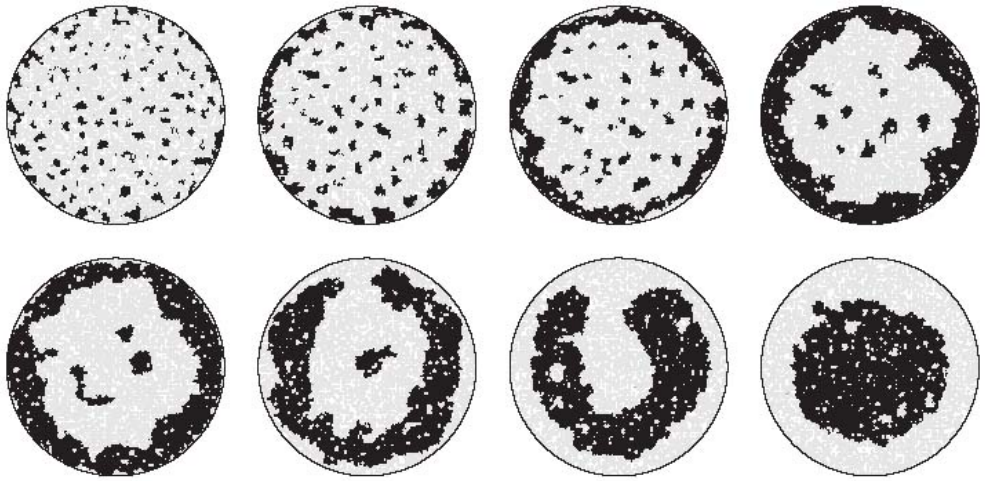

Fig. 2 – Time sequence of MC configurations of the contact area for the potential ranges $z_s = 1.0$, $z_r = 1.6$ and concentrations $a^2 X_s = 0.1$, $a^2 X_r = 0.5$ of stickers and repellers. Stickers are shown in black, repellers in grey. Due to the diffusion of stickers into the contact area, clusters at the rim grow faster, forming rings at intermediate time scales. The final configuration represents the equilibrium state. The snaphots are taken at 10^3, $4 \cdot 10^3$, 10^4, $4 \cdot 10^4$, $1.6 \cdot 10^5$, $6.3 \cdot 10^5$, 10^6, and $4 \cdot 10^6$ MC steps.

with the substrate or opposing membrane. Thus, the whole membrane is a circle of diameter $200a$. The stickers and repellers are free to diffuse within the entire membrane, but interact with the substrate or opposing membrane only in the contact area. This mimics the adhesion geometry of a spherical vesicle or cell, with a ratio of 1 : 4 between contact area and overall membrane area. We assume that this geometry is established during an initial adhesion event which is fast compared to the pattern formation described below. This assumption seems to be justified both for the biomimetic vesicles studied in ref. [7] and for T cells [2]. In the first case, the considered geometry arises from initial gravity-induced adhesion of the vesicles on the substrate. In the case of T cells, initial adhesion is mediated by relatively long integrin molecules. Together with the glycocalyx, the integrin complexes impose a barrier to the subsequent binding of the shorter TCR-MHC complexes [5] which correspond to the stickers in our model.

Our MC simulations start from a random distribution of stickers and repellers, and a rescaled membrane separation $z_i \equiv (l_i/a)\sqrt{\kappa/T} = z_r$ in the contact area, with all stickers unbound. A Monte Carlo step consists in attempts i) to move each sticker and repeller to one of the 8 neighbor sites and ii) to shift the rescaled membrane separation z_i at every lattice site i in the contact area. In this way, we incorporate the lateral diffusion within the membrane and use a Rouse-type dynamics for its shape fluctuations [16]. Within the contact area, the maximal wavelength of these fluctuations is small and one may ignore hydrodynamic interactions which determine the relaxation times in the long-wavelength limit. We assume that the on-rate for sticker binding is large and that the stickers bind fast compared to membrane relaxation times. A local membrane move which brings a sticker within the potential range z_s then leads immediately to sticker binding. The off-rate for sticker unbinding is small for the high binding energies considered here.

Regime (A): At large repeller ranges z_r or small sticker concentrations X_s, we find that adhesion proceeds by growth of a single nucleus of bound stickers (MC configurations not shown). This adhesion behavior has been experimentally observed for biomimetic vesicles with integrins as stickers and anchored polymers as repellers [7].

Regime (B): In fig. 2, a typical time sequence of MC configurations is shown for the rescaled

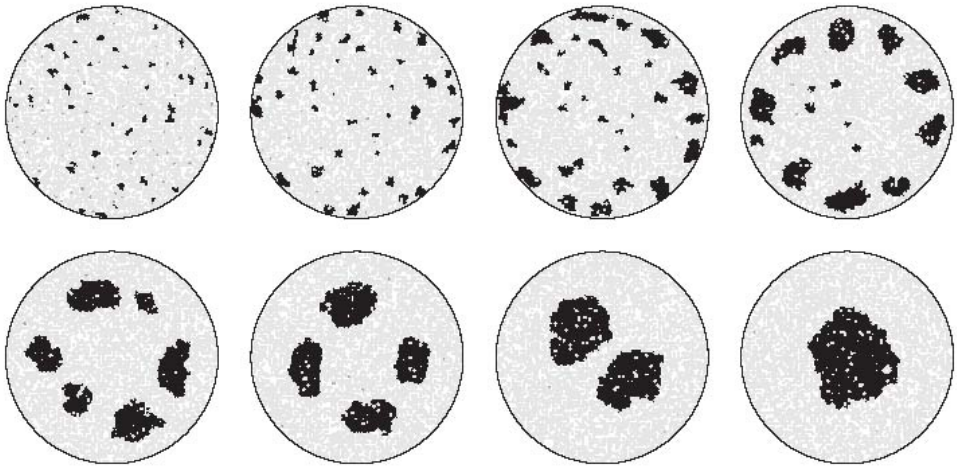

Fig. 3 – Time sequence of MC configurations of the contact area for the potential ranges $z_s = 1.0$, $z_r = 1.8$ and concentrations $a^2 X_s = 0.04$, $a^2 X_r = 0.5$ of stickers and repellers. Stickers are shown in black, repellers in grey. The sticker concentration is smaller than in fig. 2, which results in circular patterns of separate clusters at intermediate times, instead of closed sticker rings as in fig. 2. The snaphots are taken at 10^3, $4 \cdot 10^3$, $1.6 \cdot 10^4$, $6.3 \cdot 10^4$, $4 \cdot 10^5$, $6.3 \cdot 10^5$, $1.6 \cdot 10^6$, and $4 \cdot 10^6$ MC steps.

potential ranges $z_s = 1.0$, $z_r = 1.6$ and overall sticker and repeller concentrations $a^2 X_s = 0.1$, $a^2 X_r = 0.5$. Initially, the stickers bind at many nucleation sites and form small clusters, see the first configuration of the contact area in fig. 2. Due to the sticker inflow from the non-adhesive membrane around the contact area, sticker clusters at the rim of this area grow faster, and after cluster coalescense, a ring of bound stickers is formed, enclosing trapped repellers and remaining small sticker clusters in the center of the contact area. At later times, this pattern is inverted, and finally, a single central sticker cluster emerges which is surrounded by a ring of repellers. This final configuration minimizes the line tension between the bound and unbound membrane domains and, therefore, represents the equilibrium state. Rather similar patterns involving an intermediate ring of TCR-MHC complexes and a final central disk of these complexes have been observed during T cell adhesion [2].

Regime (C): MC configurations of the contact area at the smaller sticker concentration $a^2 X_s = 0.04$ and slightly larger repeller range $z_r = 1.8$ are shown in fig. 3. Initially, many sticker clusters are again formed in nucleation events, and subsequently, sticker clusters at the edge of the contact area grow faster due to the diffusion of stickers into the contact area. But in contrast to the previous situation, the sticker concentration is not large enough for the formation of a closed ring of bound stickers at intermediate times. Instead, a ring of several disconnected clusters emerges. The clusters eventually coalesce to form the equilibrium configuration with one central sticker cluster.

The different regimes (A), (B), and (C) for pattern formation can be systematically characterized in terms of two quantities. The first quantity is the maximal number of bound sticker clusters N_{cl}^{max} attained during the time course of a simulation. In fig. 4(a), the number of bound sticker clusters N_{cl} is displayed as a function of time for the same parameters as in fig. 3. After initial increase due to nucleation events, the cluster number N_{cl} attains the maximal value $N_{cl} = N_{cl}^{max}$, and later decreases as a consequence of cluster coalescence. Another characteristic quantity is the maximal sticker occupation Y^{max} for the ring of the contact area. To define the latter quantity, we consider the membrane ring with distances $40a < r < 50a$ from the center of the contact area, divide it into 100 equal segments, each

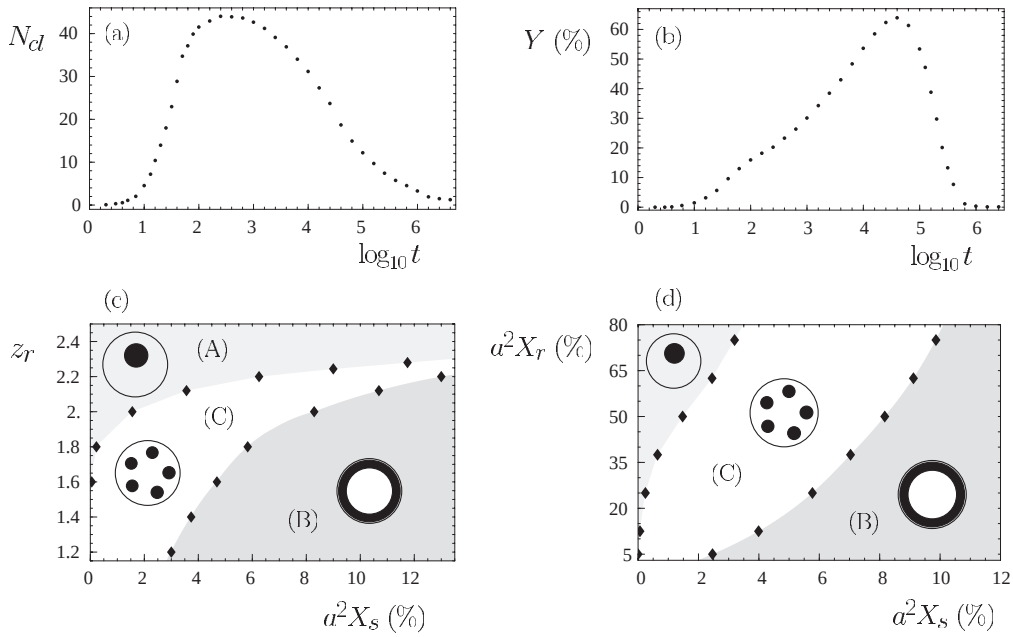

Fig. 4 – (a) Number of bound sticker clusters $N_{\rm cl}$ and (b) sticker occupation Y of the contact area ring with distances $40a < r < 50a$ from the center as a function of the time t in MC steps for the same parameters as in fig. 3. The data are averages from 24 independent simulations. (c), (d) Dependence of the dynamic regimes (A), (B), and (C) on the sticker and repeller concentrations $X_{\rm s}$ and $X_{\rm r}$ and the repeller range $z_{\rm r}$ for the sticker potential range $z_{\rm s} = 1.0$. The repeller concentration is given by $a^2X_{\rm r} = 0.5$ in (c), and the repeller range is $z_{\rm r} = 2.0$ in (d). Characteristic patterns are indicated for all three regimes. In the upper left grey area, the maximal number of sticker clusters $N_{\rm cl}^{\rm max}$ during adhesion is smaller than 3. In the lower right grey area, the maximal value $Y^{\rm max}$ for the ring occupation is larger than 0.8.

covering an angle $2\pi/100$, and determine the fraction of segments Y which contain bound stickers. The ring occupation Y has a similar time evolution as $N_{\rm cl}$, with a maximal value $Y^{\rm max}$ at intermediate times where a ring of sticker clusters is formed, and a final decrease to zero as the equilibrium conformation is approached, see fig. 4(b). We find that appropriate values to describe the crossover between the three dynamic regimes are given by $N_{\rm cl}^{\rm max} = 3$ and $Y^{\rm max} = 0.8$: Simulations with $Y^{\rm max} > 0.8$ show intermediate configurations with a closed ring of bound stickers as in fig. 2. For $N_{\rm cl}^{\rm max} < 3$, on the other hand, adhesion proceeds by sticker condensation mostly around a single, dominant nucleus. For $N_{\rm cl}^{\rm max} > 3$ and $Y^{\rm max} < 0.8$, configurations with a circular arrangement of separate clusters emerge as in fig. 3.

The dynamic behavior just described can be understood in terms of the nucleation time $\tau_{\rm nuc}$ for the formation of bound sticker clusters, compared to typical diffusion times of the stickers. The nucleation time $\tau_{\rm nuc}$ critically depends on the strength of the repeller barrier which opposes sticker binding. A membrane segment with linear extension L thermally fluctuates with a typical out-of-plane deviation $L_\perp \sim L\sqrt{T/\kappa}$. A segment crossing the barrier region between $l_{\rm r}$ and $l_{\rm s}$ therefore has a typical area $A \sim (\kappa/T)(l_{\rm r} - l_{\rm s})^2$ and activation energy $\Delta E_{\rm ba} \simeq U_{\rm ba} A/a^2$, where $U_{\rm ba} \simeq T \ln(1 + e^{\mu_{\rm r}/T})$ is the height of the energy barrier, see eq. (3). The nucleation probability $P_{\rm nuc}$ therefore scales as $P_{\rm nuc} \sim \exp[-\Delta E_{\rm ba}/T]$. The nucleation time $\tau_{\rm nuc}$ is proportional to $1/P_{\rm nuc}$, and scales as $\tau_{\rm nuc} \sim \exp[c'\kappa U_{\rm ba}(l_{\rm r} - l_{\rm s})^2/(a^2T^2)]$, where c' is a dimensionless coefficient. Since the unbound stickers perform a random walk on the lattice, the diffusion time $\tau_{\rm dif}$ to cover a typical distance such as the diameter D of the contact

area simply scales as $\tau_{\rm dif} \sim D^2$. In contrast, the nucleation time $\tau_{\rm nuc}$ strongly increases with increasing repeller range $l_{\rm r}$ or barrier height $U_{\rm ba}$, which also leads to an increase of the regime (A) where adhesion proceeds via diffusive growth of a single, dominant nucleus, see fig. 4(c). The barrier height $U_{\rm ba}$ depends on the chemical potential $\mu_{\rm r}$ or the concentration $X_{\rm r}$ of the repellers, see above. For smaller repeller range $l_{\rm r}$ or concentration $X_{\rm r}$, many nuclei are formed, which leads to the dynamic regimes (B) and (C), depending on the sticker concentration $X_{\rm s}$ and on the line tension between the sticker and repeller domains. Within our MC simulations, the ratio $\tau_{\rm nuc}/\tau_{\rm dif}$ also depends on the relative frequency with which we attempt to change the separation field z and the concentration field n and which was chosen to be one. According to our scaling arguments, other choices for this relative frequency may lead to a shift of the boundaries between the three regimes, but not to a qualitatively different adhesion behavior.

Conclusions. – In summary, we have shown that the various domain patterns which have been observed during the sticker-mediated adhesion of membranes can be understood within a unified theoretical framework. This framework is based i) on lateral phase separation due to a repeller barrier opposing sticker binding and ii) on the nucleation of the bound sticker domains. It is instructive to use our theoretical results in order to estimate the strength of the repeller barrier in the case of T cells. For small repeller concentrations with $a^2 X_{\rm r} \ll 1$, the effective barrier height $U_{\rm ba} = T \ln(1 + e^{\mu_{\rm r}/T})$ in eq. (3) can be written as $U_{\rm ba} \simeq T e^{\mu_{\rm r}/T} \simeq T a^2 X_{\rm r}$. According to eq. (3), lateral phase separation then occurs for $X_{\rm r}(l_{\rm r} - l_{\rm s})^2 > cT/\kappa$ with $c \simeq 0.013$. For T cells, the length of the TCR-MHC complexes corresponding to the stickers in our model is 15 nm [5]. Taking the typical values $l_{\rm r} \simeq 40$ nm and $X_{\rm r} \simeq 50/\mu{\rm m}^2$ for the repellers [2, 5, 6] and $\kappa \simeq 20\ T$ for the bending rigidity of lipid membranes leads to a repeller barrier clearly above the critical strength. Therefore, the barrier mechanism for lateral phase separation provides a possible explanation for the observed aggregation of the TCR-MHC complexes and for the pattern formation found in experiments.

REFERENCES

[1] Monks C. R. F., Freiberg B. A., Kupfer H., Sciaky N. and Kupfer A., *Nature*, **395** (1998) 82.
[2] Grakoui A., Bromley S. K., Sumen C., Davis M. M., Shaw A. S., Allen P. M. and Dustin M. L., *Science*, **285** (1999) 221.
[3] Davis D. M., Chiu I., Fassett M., Cohen G. B., Mandelboim O. and Strominger J. L., *Proc. Natl. Acad. Sci. USA*, **96** (1999) 15062.
[4] Wülfing C. and Davis M. D., *Science*, **282** (1998) 2266.
[5] Dustin M. L. and Cooper J. A., *Nat. Immunol.* **1** (2000) 23.
[6] Qi S. Y., Groves J. T. and Chakraborty A. K., *Proc. Natl. Acad. Sci. USA*, **98** (2001) 6548.
[7] Boulbitch A., Guttenberg Z. and Sackmann E., *Biophys. J.*, **81** (2001) 2743.
[8] Lipowsky R., *Phys. Rev. Lett.,* **77** (1996) 1652.
[9] Weikl T. R. and Lipowsky R., *Phys. Rev. E*, **64** (2001) 011903.
[10] Lipowsky R., *J. Phys. II*, **4** (1994) 1755; Ammann A. and Lipowksy R., *J. Phys. II*, **6** (1996) 255.
[11] Weikl T. R., Netz R. R. and Lipowsky R., *Phys. Rev. E*, **62** (2000) R45.
[12] Weikl T. R., *Europhys. Lett.*, **54** (2001) 547.
[13] Komura S. and Andelman A., *Eur. Phys. J. E*, **3** (2000) 259.
[14] Bruinsma R., Behrisch A. and Sackmann E., *Phys. Rev. E*, **61** (2000) 4253.
[15] Weikl T. R., Andelman D., Komura S. and Lipowsky R., *Eur. Phys. J. E*, **8** (2002) 59.
[16] Lipowsky R. and Zielinska B., *Phys. Rev. Lett.*, **62** (1989) 1572.